Proceedings World Geothermal Congress 2020+1
Reykjavik, Iceland, April - October 2021

Permeability Evolution of Fractured Granite due to Pressure Solution and Free-face Dissolution in Superhot Geothermal Environments

Noriaki Watanabe[1,*], Kohei Saito[1], Atsushi Okamoto[1], Noriyoshi Tsuchiya[1], Takeshi Komai[1], Takuya Ishibashi[2], Hanae Saishu[2] and Norihiro Watanabe[2]

[1]Department of Environmental Studies for Advanced Society, Graduate School of Environmental Studies, Tohoku University

[2]Fukushima Renewable Energy Institute, National Institute of Advanced Industrial Science and Technology (AIST)

[*]noriaki.watanabe.e6@tohoku.ac.jp

Keywords: permeability, fracture, pressure solution, free-face dissolution, supercritical water, enhanced geothermal system

ABSTRACT

Superhot geothermal environments in high temperature ductile granitic crusts of ca. 400-500°C and 2-4 km depths are recognized as a frontier of geothermal energy. In developing such environments, hydraulic fracturing is a promising way to create or recreate permeable fracture networks (i.e., geothermal reservoirs) to effectively access the geothermal energy frontier with the concept of enhanced geothermal systems (EGS). However, there is a concern about the possibility to stabilize/enhance the permeability created by hydraulic fracturing because pressure solution may reduce permeability after pore water pressure/effective confining stress returns to the original lower/higher level. On the other hand, permeability may be enhanced by free-face dissolution even if pressure solution occurs. However, the rates of permeability reduction by pressure solution and permeability enhancement by free-face dissolution have not been fully understand for the superhot geothermal environments, and the possibility to stabilize/enhance permeability has therefore been unclear. We present the results of a set of hydrothermal flow-through experiments on 400°C fractured granite samples at various effective confining stresses and clarify influences of stress level and plasticity of the fracture on the rate of permeability change by pressure solution. Additionally, we present results of another set of hydrothermal flow-through experiments on 400°C fractured granite samples at various pore water pressures and clarify influences of pore water pressure and corresponding mineral solubility on the rate of permeability change by free-face dissolution. Finally, based on the experimental results, the rates of permeability changes by pressure solution and free-face dissolution are modeled respectively as functions of effective confining stress and quartz solubility. The present study suggests that permeability may be stabilized or enhanced in superhot EGS even under the presence of pressure solution by keeping a difference between a concentration of pore water and solubility for quartz higher than a stress-dependent permeability stabilization criterion.

1. INTRODUCTION

Geothermal systems operating at 150–300°C have been used for electric power generation for over 100 years. Accessing unexploited deeper and hotter geothermal environments exceeding the critical temperature of water (374°C for pure water and 406°C for seawater) at depths of ca. 2-4 km could result in increased productivity as well as sustainability because superhot or supercritical geothermal environments such as those demonstrated by drilling in Italy (Baron and Ungemach, 1981; Batini et al., 1983; Ruggieri and Gianelli, 1995), Iceland (Steingrimsson et al., 1990; Friðleifsson et al., 2014; Friðleifsson and Elders, 2017), the United States (Fournier, 1991; Garcia et al., 2016), Mexico (Espinosa-Paredes and Garcia-Gutierrez, 2003) and Japan (Kato et al., 1998) could produce superheated steam or supercritical water having very high specific enthalpies of ≥ approximately 2 MJ/kg (Smith and Shaw, 1975 and 1978; Friðleifsson and Elders, 2005; Tester et al., 2006; Friðleifsson et al. 2007; Elders et al., 2014). For instance, the well tests on the IDDP-1 well in Iceland achieved flowrates of up to 50 kg s^{-1} at temperatures of up to 440°C (Ingason et al., 2014). At such high enthalpies (~3.2 MJ kg−1), sustained flowrates of ~30 kg s^{-1} could generate ~20 MWe which is an order of magnitude larger than the electric power typically obtained from a conventional geothermal well in Iceland.

In the continental granitic crust, the transition to superhot geothermal environments above approximately 400°C occurs near the brittle–ductile transition zone (Fournier, 1999). Key aspects of these superhot environments include the increased efficiency of crystal plastic processes (Tullis and Yund, 1977; Violay et al. 2017), the retrograde solubility of quartz (Fournier, 1991; Saishu et al. 2014; Tsuchiya and Hirano, 2007) and increased rates of healing and sealing of fractures by water-rock interactions (Moore et al. 1994; Morrow et al., 2001). All of these characteristics could result in the loss of the network of permeable fractures that store and transmit geothermal fluids. These networks, however, are likely to form and persist for a certain period (Tsuchiya et al., 2016; Watanabe et al., 2017a; Weis et al., 2012). It is therefore worthwhile to develop enhanced geothermal system (EGS) technologies such as hydraulic fracturing to create or recreate networks of permeable fractures through which water circulates between injection and production wells (Li et al., 2019) suitable for the superhot geothermal environments (Reinsch et al., 2017).

Recently, laboratory experiments on hydraulic fracturing on granite involving the application of low-viscosity water to granite at temperatures ≥400°C under triaxial stress have demonstrated the formation of a network of permeable microfractures densely distributed throughout the entire rock body, producing a so-called cloud-fracture network (Watanabe et al., 2017b and 2019). The fracturing was found to be initiated at a relatively low injection pressure between the intermediate and minimum principal stresses, and propagated following the distribution of preexisting microfractures, independent of the directions of the principal stresses. It has been therefore confirmed that hydraulic fracturing can create excellent fracture patterns that should allow the effective extraction of thermal energy in superhot geothermal environments. However, there is a concern about the sustainability of the permeability of the fractures thus created because previous studies have suggested that permeability may decrease over time due to pressure solution of

the fracture surfaces, although it has also been suggested that permeability may increase over time due to free-face dissolution of the fracture surfaces.

There are two mechanisms in the pressure solution process, namely stress solution and strain solution, that may lead to the reduction of fracture apertures and corresponding permeability (Shimizu, 1995; Figure 1). Stress solution occurs at the loaded faces of bridging asperities within a fracture and is driven by a difference in stress level between the loaded face and the other (free) face. On the other hand, strain solution occurs at the edges of bridging asperities, and is driven mainly by plastic strain energy, where the influence of strain solution is usually neglected because it is believed to be small.

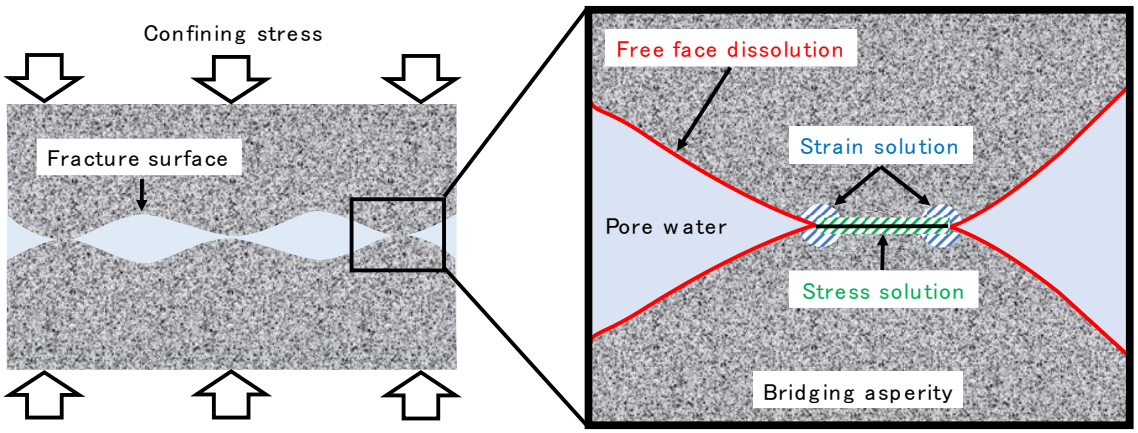

Figure 1: Locations where pressure solution (stress and/or strain solution) and free-face dissolution occur within water-filled fracture in rock subjected to confining stress.

Consequently, the mass flux created by pressure solution (i.e., stress solution) M_{ps} (kg m^{-2} s^{-1}) is usually expressed as (Rutter, 1976; Yasuhara et al., 2003 and 2004; Ishibashi et al., 2013):

$$M_{ps} = \frac{3\rho {V_m}^2}{RT} k_+ \left(\frac{\sigma - P_p}{R_c} - \sigma_{crit} \right) = \frac{3\rho {V_m}^2}{RT} k_+ \left(\frac{\sigma_{eff}}{R_c} - \sigma_{crit} \right), \quad (1)$$

where ρ (kg/m^3) and V_m (m^3 /mol) respectively are the density and molar volume of the solid, R (J K^{-1} mol^{-1}) is the gas constant, and T is the temperature (K), k_+ (mol m^{-2} s^{-1}) is the dissolution rate constant for the solid, σ (Pa) is the confining stress, P_p (Pa) is the pore water pressure (Pa), σ_{eff} (Pa) is the effective confining stress, σ_{crit} (Pa) is the critical stress that defines the normal stress level where the shortening of the asperity will effectively halt, R_c (-) is the contact area ratio for the fracture plane. The critical stress is expressed as (Revil, 1999; modified from Stephenson et al., 1992):

$$\sigma_{crit} = \frac{E_m \left(1 - \frac{T}{T_m}\right)}{4V_m} \quad (2)$$

where E_m (J mol^{-1}) and T_m (K) are the heat and temperature of fusion for the solid, respectively (e.g., E_m = 8.57 kJ mol^{-1}, T_m = 1883 K for quartz). However, the impact of strain solution has not been clarified and, therefore, the rate at which the permeability drops may be changed by the onset of plastic deformation of the fracture. It has recently been discovered that plastic deformation of a fracture in granitic rocks occurs at effective confining stresses higher than the temperature-dependent elastic-plastic transition stress $\sigma_{eff,\,trans}$ (Pa) expressed by the following equation (Watanabe et al., 2017a):

$$\log_{10}\sigma_{eff,tans} = 12.8 - 4.3\log_{10}(T - 273.15) \quad (3)$$

Indeed, accelerated reduction of permeability by the elastic-plastic transition can be inferred from the results obtained by Moore et al. (1994) and Morrow et al. (2001). The results of hydrothermal flow-through experiments on granite at 150-500°C with a confining stress of 150 MPa and a pore water pressure of 100 MPa (i.e., effective confining stress of 50 MPa) indicate a permeability reduction with time at all temperatures. They defined the slope of the relation between the logarithmic value of the permeability k (m^2) and time t (days) as a rate of permeability change r (days^{-1}) as follows:

$$r = \frac{\Delta \log_{10} k}{\Delta t} \quad (4)$$

The relationship between the rate of permeability reduction and the temperature has been reported by Morrow et al. (2001), and the reduction rate seems to increase with increasing temperature. However, a jump in the reduction rate seems to be present between 350°C and 400°C. At the given effective confining stress of 50 MPa, 350°C and 400°C, respectively, correspond to the elastic and plastic conditions based on Eq. (3), suggesting acceleration of permeability reduction due to strain solution in addition to stress solution in superhot geothermal environments within ductile granitic crusts. However, this point has not been clear because the previous experiments were not designed to investigate permeability changes solely brought about by pressure solution, and, of course, the influence of the recently discovered elastic-plastic transition stress.

On the other hand, free-face dissolution proceeds at the free faces of fracture surfaces (Figure 1), and may increase the aperture size and therefore the permeability of the fracture. The mass flux by free-face dissolution M_{ffd} (kg m^{-2} s^{-1}) may be written as (Yasuhara et al., 2006; Ishibashi et al., 2013):

$$M_{ffd} = \rho V_m k_+ \left(1 - \frac{C_{pore}}{C_{eq}}\right) \quad (5)$$

where C_{pore} (kg kg^{-1}) and C_{eq} (kg kg^{-1}) are the concentration of the pore water and the solubility of the solid, respectively. More intense free-face dissolution is expected to proceed at higher temperatures due to a larger reaction rate constant and higher pore pressure due to higher mineral solubility. Therefore, at the high temperatures and high pore pressures expected in superhot geothermal environments, there is also a possibility that permeability may be enhanced due to free-face dissolution, the influence of which is perhaps comparable to that of pressure solution. In Okamoto et al. (2017), for instance, an increase in permeability over time was observed for fractures in granite in hydrothermal flow-through experiments at 350°C with a confining stress of 40 MPa and a pore water pressure of 20 MPa (i.e, effective confining stress of 20 MP). The direction (increase or decrease) and rate of permeability change is the result of competition between pressure solution and free-face dissolution. However, no experiment has been conducted to separately evaluate the rates of permeability change by free-face dissolution and pressure solution, so further consideration of the sustainability of permeability in superhot geothermal environments has not yet been possible.

In this context, the objectives of the present study are to clarify the relative magnitudes of the rates of permeability change by pressure solution and free-face dissolution for fractures of granite in enhanced geothermal systems created in superhot geothermal environments, and to clarify the possibility of and means for stabilizing/enhancing the permeability via mapping the conditions in which permeability enhancement and reduction occur in fractures. We conducted a set of hydrothermal flow-through experiments on 400°C fractured granite samples at various effective confining stresses with a low-pressure steam to suppress free-face dissolution. Based on the results of these experiments, we discuss the influences of stress level and fracture plasticity on the rate of permeability change brought on by pressure solution. Additionally, we conducted another set of hydrothermal flow-through experiments on fractured granite samples at 400°C and various pore water pressures with a low effective confining stress to suppress pressure solution and discuss the influences of pore-water-pressure-dependent mineral solubility on the rate of permeability change caused by free-face dissolution. Moreover, the rates of permeability change by pressure solution and free-face dissolution are modeled respectively as functions of effective confining stress and mineral solubility. Finally, a permeability stabilization criterion at 350-500°C is defined to reveal the possibility and means of stabilizing or even enhancing permeability in superhot EGS.

2. EXPERIMENTAL METHODS

2.1 Experimental Sample

Cylindrical granite samples (diameter: 30 mm, length: 25 mm), containing a single tensile fracture induced by splitting a larger notched granite block with a wedge, were prepared using Inada granite from Ibaraki prefecture, Japan (Figure 2a). The Young's modulus, porosity and permeability of Inada granite at or near atmospheric pressure are, respectively, approximately 55–80 GPa, 0.5–0.8% and 2×10^{-18}–8×10^{-18} m^2 (Watanabe et al., 2017b and 2019). The modal composition of the major component minerals measured using a point counter is 36% quartz, 32% plagioclase, 28% alkali-feldspar and 4% biotite (Lin, 2002). As accessory minerals, allanite, zircon, apatite, ilmenite, etc., occur in the rock. It is a medium-grained granite, and the grain sizes of the quartz, plagioclase, alkali-feldspar and biotite are approximately 3-4 mm, 2-3 mm, 2-4 mm and 1-3 mm, respectively.

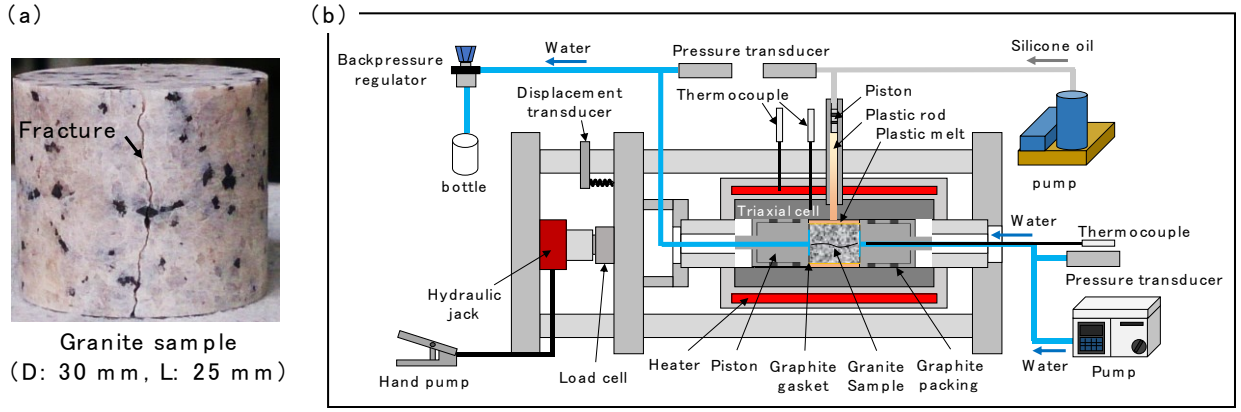

Figure 2: (a) Experimental sample and (b) system for hydrothermal flow-through experiment.

2.2 Experimental System

An experimental system developed by Watanabe et al. (2017a) was used for the hydrothermal flow-through experiments (Figure 2b). The novelty of this system is the use of a special triaxial cell, which uses a high-viscosity plastic melt as a confining fluid and a thin plastic film as a sleeve. The plastic melt is composed of PEEK (polyether ether ketone), which has a melting point of 343°C and a decomposition temperature greater than 538°C. Because of its high viscosity of 350 Pa s even at 400°C, sealing the PEEK melt is easy. The plastic film is polyimide (thickness: ca. 50 μm), which has no melting point (that is, it decomposes before melting) and a high decomposition temperature of >500°C. It also acts as a release agent after the experiment. This triaxial cell can work at ca. 350-500°C when using PEEK and at lower temperatures with a plastic that has a lower melting point, such as polyethylene.

The sample, wrapped in the polyimide film, is first placed inside a PEEK cylinder within a tri-axial cell. Graphite gaskets having holes for fluid flow are attached at both ends of the sample. A tube containing a PEEK rod, which is used to inject the PEEK melt, is attached to the upper part of the cell. The cell is then placed within an electric furnace. At a small axial pressure of about 2 MPa, maintained by a hydraulic jack, the temperature is increased to a prescribed value (400°C in the present study), melting both the PEEK cylinder and the rod inside the triaxial cell. Temperatures are measured both inside and outside the cell. A prescribed confining

stress is then applied to the sample by adjusting the confining pressure through the PEEK melt; the axial pressure is slightly higher than the confining pressure (the differential stress is approximately 2 MPa). The confining pressure is controlled by injecting the PEEK melt at a prescribed pressure through the upper tube, using a metallic piston that is displaced by pumping silicone oil at constant pressure. At the prescribed temperature and confining stress, pure water is injected into the sample at a prescribed flow rate (0.1 mL/min at room temperature in the present study) using a pump. It exits the sample at a prescribed water pressure controlled by a backpressure regulator, where the injected water is preheated to the prescribed temperature before entering the sample. Note that the pore water pressure in the present study was approximately equivalent to the backpressure because the difference in pressure between the inlet and outlet was small (less than 1 MPa) in all experiments. The permeability k (m^2) of the fracture contained within the sample was calculated based on the cubic law assuming a negligibly small permeability of the rock matrix (Witherspoon et al., 1980; Tsang and Witherspoon, 1981):

$$k = \frac{a_h^2}{12} \tag{6}$$

In this expression, a_h (m) is the hydraulic aperture, which can be calculated from the following equation:

$$a_h = \left(\frac{12\mu LQ}{W\Delta P}\right)^{\frac{1}{3}} \tag{7}$$

where Q (m^3/s) is the flow rate of water, ΔP (Pa) is the differential pressure between the inlet and outlet, μ (Pa s) is the viscosity of water, and L (m) and W (m) are, respectively, the apparent lengths of the fracture in the directions parallel and perpendicular to the macroscopic flow direction (i.e., the length and diameter of the sample in the present study).

In the present experiments, the pressures were recorded every minute. However, we discuss changes in permeability using improved differential pressure data smoothed via 10-point (10-minute) adjacent averaging. This smoothing was done to remove unessential fluctuations in the differential pressure originating from the use of the backpressure regulator. The effluent was collected during each experiment, and was analyzed for average concentrations of Si, Al, Ca, Na, K, Fe and Mg by inductively coupled plasma optical emission spectrometry (ICP-OES) to investigate occurrences of pressure solution and free-face dissolution.

2.3 Experimental Condition

The set of experiments for pressure solution was conducted at effective confining stresses (confining stresses) of 5 (15), 18 (28), 30 (40), 40 (50) and 50 (60) MPa with a low backpressure (i.e., pore water pressure) of 10 MPa. The elastic-plastic transition stress at 400°C is about 40 MPa based on Eq. (3). We therefore refer to effective stress conditions of < 40 MPa and ≥ 40 MPa, respectively, as the elastic and plastic conditions. On the other hand, another set of experiments for free-face dissolution was conducted at pore water pressures of 10 (vapor condition), and 25 and 35 MPa (supercritical condition) with a low effective confining stress of 5 MPa, where the corresponding confining stresses were therefore 15, 30 and 40 MPa respectively.

3. RESULTS AND DISCUSSION

3.1 Permeability change due to pressure solution

Figure 3 shows changes in permeability with time at effective confining stresses of 5, 18, 30, 40 and 50 MPa. Temperature and pore water pressure were identical at all stress levels (i.e., 400°C and 10 MPa). The reactivity of the water was therefore identical in all conditions, where quartz solubility, for instance, was very low at around 4 mg/kg (Manning, 1994). At all stress levels, the permeability repeatedly increased and decreased over a short time range, implying that competition between permeability enhancement and reduction occurred even when pressure solution was likely to be the predominant reaction. For instance, temporal permeability enhancement may occur by pressure solution only if parts of the bridging asperities are shortened to create new apertures. On the other hand, overall changes clearly depended on the stress level as discussed below.

At effective confining stresses of 5 and 18 MPa (elastic condition), permeability increased slightly at the lower confining stress but was almost independent of time at the higher stress. Note that the differential pressure at 18 MPa could not be obtained during the period from about 0.1 to 0.3 days due to trouble in the recording system, but the experiment was not stopped during that time, and ultimately continued for 0.6 days. As described before, Moore et al. (1994) and Morrow et al. (2001) defined the slope of the relation between the logarithmic value of the permeability k (m^2) and time t (days) as the rate of permeability change r ($days^{-1}$). Applying this definition (Eq. 4) in the present study, the rate of permeability change was found to be 1.7×10^{-2} day^{-1} at 5 MPa and 4.7×10^{-3} day^{-1} at 18 MPa. On the other hand, at an effective confining stress of 30 MPa, which also corresponds to the elastic condition, permeability decreased slightly with time, and the rate of permeability change is -2.2×10^{-2} $days^{-1}$. At effective stresses of 40 and 50 MPa, which correspond to the plastic condition, permeability decreased over time at higher rates (-6.5×10^{-2} day^{-1} at 40 MPa, -8.7×10^{-2} day^{-1} at 50 MPa). These observed rates of permeability reduction are within the range of 10^{-4}-10^{-1} $days^{-1}$ reported by Moore et al. (1994) and Morrow et al. (2001). Clearly, the rate of permeability change is stress-dependent, and the rate of permeability reduction increases with increasing effective confining stress, indicating the occurrence of pressure solution.

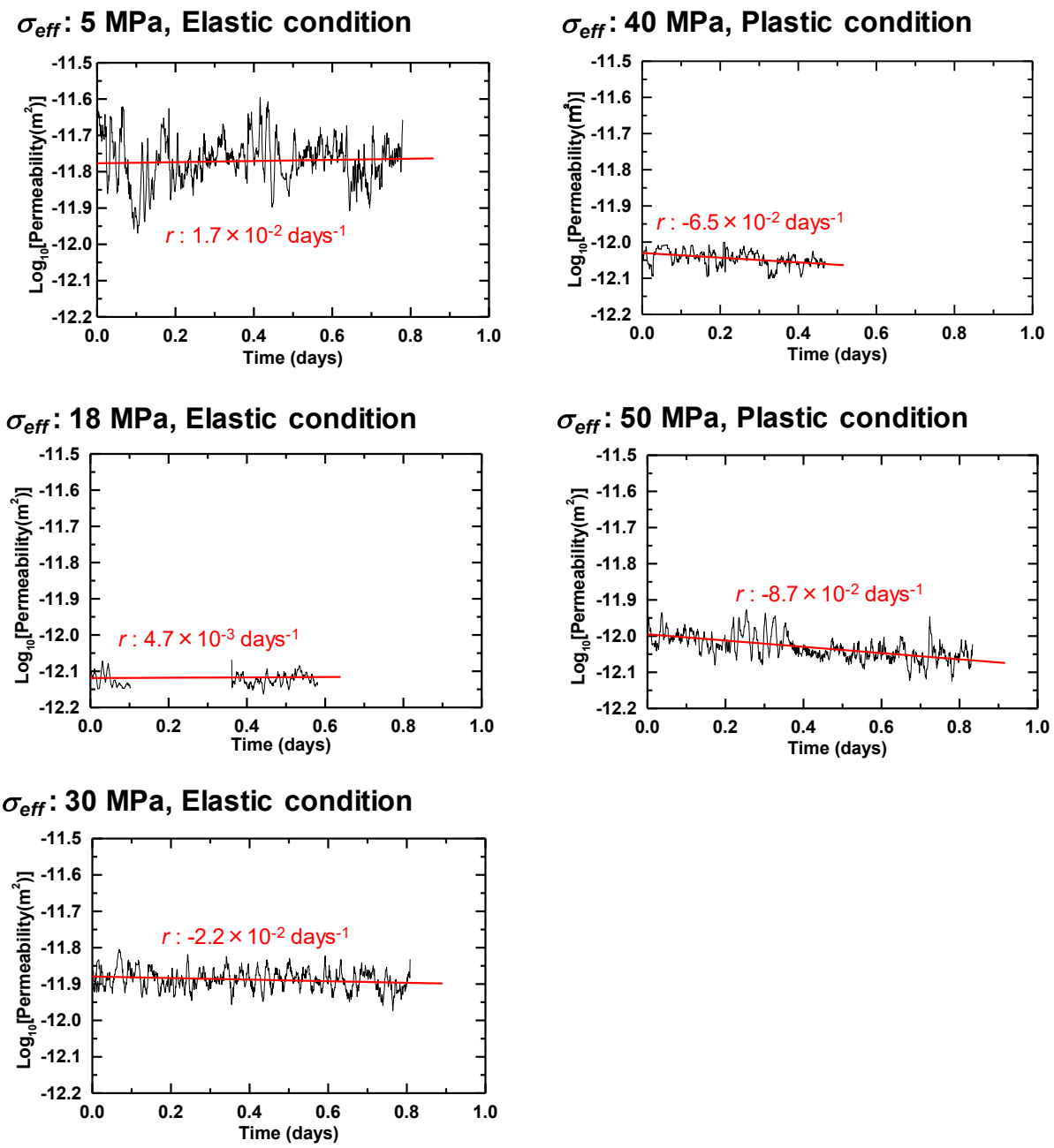

Figure 3: Changes in permeability in pressure solution experiments. Red lines are linear regression curves (least squares method).

Figure 4 shows the Si concentration of the effluent at each effective confining stress. Unfortunately, the concentrations for 40 MPa could not be obtained because the effluent analysis failed, and Fe and Mg concentrations are almost zero. The Si concentration is also clearly stress-dependent, and is larger at higher effective confining stresses, supporting the occurrence of pressure solution. On the other hand, the concentrations of the other elements are much smaller, almost negligible, and not stress dependent. This indicates preferential dissolution of quartz, which is consistent with the fact that in the temperature range of 200-300°C quartz is most stable and shows the lowest dissolution rate; at temperatures above 300°C, however, quartz has the highest dissolution rate. Alkali-feldspar and plagioclase show a negative temperature dependence above 300°C (Takahashi et al., 1988). Therefore, it is natural that preferential dissolution of quartz by pressure solution occurred in the present study.

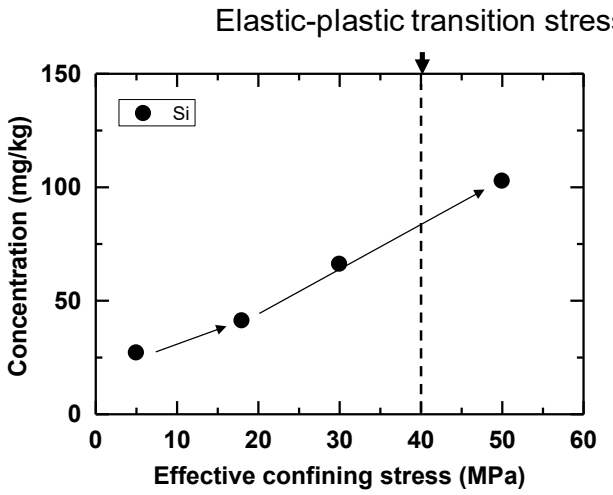

Figure 4: Stress-dependence of Si concentration in pressure solution experiments. The arrows approximate the stress dependence.

The stress dependence between 5 MPa and 18 MPa is smaller than that between 18 MPa and 50 MPa. This indicates that pressure solution effectively starts at an effective confining stress of around 20 MPa due to stress at the bridging asperities exceeding the critical stress (Eqs. 1-2). Considering that the critical stress for quartz is around 61 MPa (E_m = 8.57 kJ/mol, T_m = 1883 K), the contact area ratio was about 0.33, interestingly corresponding closely to the volumetric percentage of quartz in the granite (i.e., 36%). Also note that the linear stress dependence of the Si concentration at ≥18 MPa indicates a negligible influence of strain solution, as the elastic-plastic transition is at about 40 MPa.

Figure 5 shows the stress dependence of the rate of permeability change. As mentioned before, the rate of permeability change is stress dependent. That dependence increases significantly above 18 MPa, which is consistent with the stress dependence of the Si concentration. Additionally, permeability reduction does not occur or is very small at ≤18 MPa, and the rate at which it occurs at pressures ≥18 MPa increases linearly with increasing effective confining stress (slope: -3.0×10^{-3} days^{-1} MPa^{-1}). These findings indicate again that pressure solution starts at an effective confining stress around 20 MPa and strain solution has a negligibly small influence if it occurs at all.

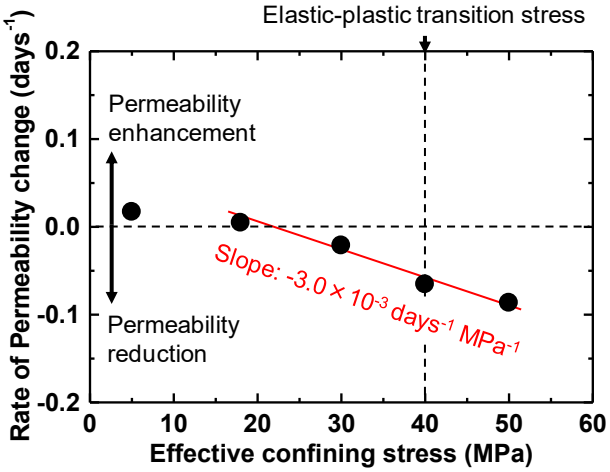

Figure 5: Stress-dependence of permeability change rate in pressure solution experiments. Red lines are linear regression curves (least squares method).

3.2 Permeability change due to free-face dissolution

Figures 6 shows how permeability change with time at pore water pressures of 10 MPa (vapor condition), 25 and 35 MPa (supercritical conditions). The temperature and effective stress were identical at all pore water pressures (i.e., 400°C and 5 MPa), where the influence of pressure solution was negligibly small at lower stress levels as discussed earlier (3.1). Only the reactivity of water, therefore, varied among the experiments, where quartz solubility, for instance, is about 4 mg/kg at 10 MPa, 85 mg/kg at 25 MPa and 798 mg/kg at 35 MPa (Manning, 1994).

At all pore water pressures, permeability repeatedly increases and decreases over a short period of time, implying that competition between permeability enhancement and reduction occurred even when free-face dissolution was likely to be the predominant reaction.

For instance, temporal permeability reduction may occur by free-face dissolution if a large quantity of bridging asperities is eroded to reduce the surface roughness needed to create apertures. Overall, permeability increased at all pore water pressures, where the rate of permeability change is 1.7×10^{-2} days^{-1} at 10 MPa, 2.7×10^{-2} day^{-1} at 25 MPa and 2.1×10^{-1} day^{-1} at 35 MPa. Clearly, the rate of permeability change is dependent on pore water pressure (i.e., factors reflecting the reactivity of water such as mineral solubility), and the rate of permeability enhancement increases with increasing pore water pressure, indicating that free-face dissolution occurs. Importantly, the rate of permeability enhancement at 35 MPa is an order of magnitude higher than the other rates, and its absolute value is larger than that of the observed rate of permeability reduction by pressure solution (Figures 3 and 5).

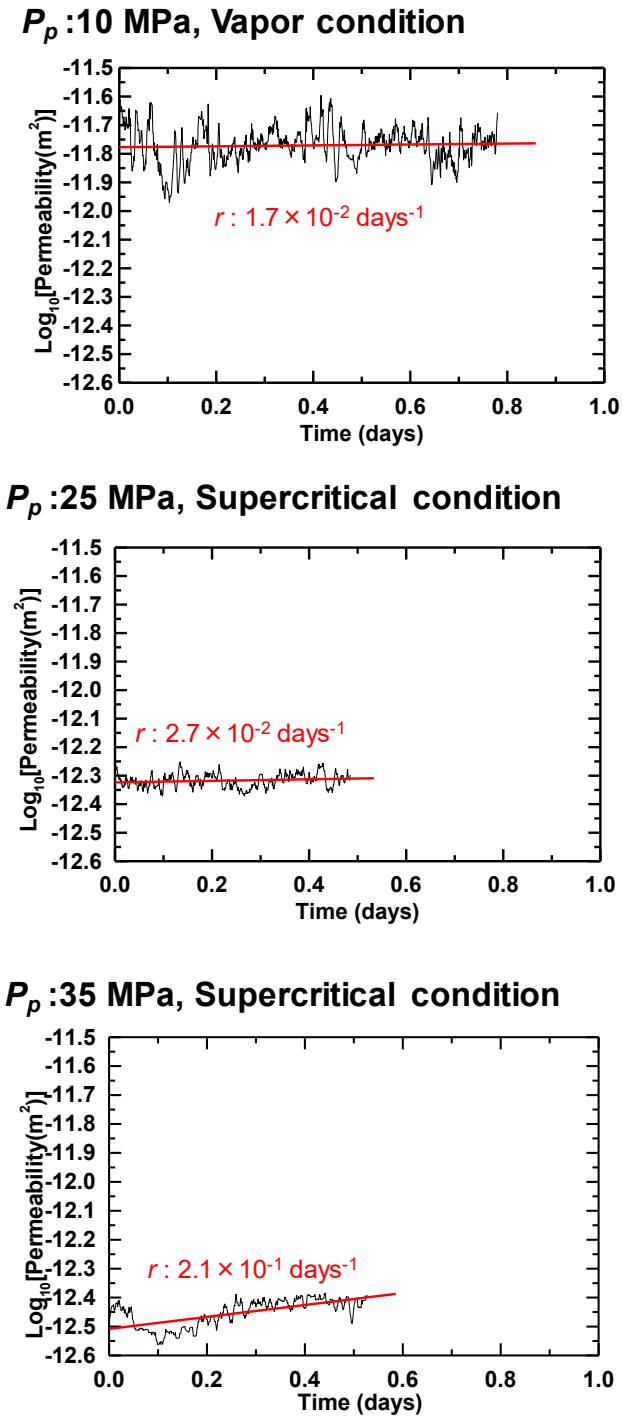

Figure 6: Changes in differential pressure and permeability in free-face solution experiments. Red lines are linear regression curves (least squares method).

Figure 7 shows the effluent's Si concentration at each pore water pressure. The Fe and Mg concentrations are almost zero. The Si concentration is clearly dependent on pore water pressure. The other elements' concentrations are generally negligible compared to Si. This indicates preferential dissolution of quartz. Indeed, estimates of the amount of quartz dissolved in the effluent from Si concentrations at each pore water pressure yield values close to the quartz solubility (Figure 8), coinciding with the fact that quartz dissolves preferentially at temperatures above 300°C as discussed before. Okamoto et al. (2017) also observed this kind of preferential

dissolution of quartz for fractures in granite in hydrothermal flow-through experiments at 350°C with a pore water pressure of 20 MPa and an effective confining stress of 20 MPa. They found that quartz dissolved preferentially, creating pockets. The other minerals acted as asperities, sustaining some fracture roughness, which is important in maintaining open fractures. Thus, it is essential to consider how the quartz solubility controls both the mass flux (Eq. 5) and the maximum amount of quartz a unit mass of water can remove from the fracture surface.

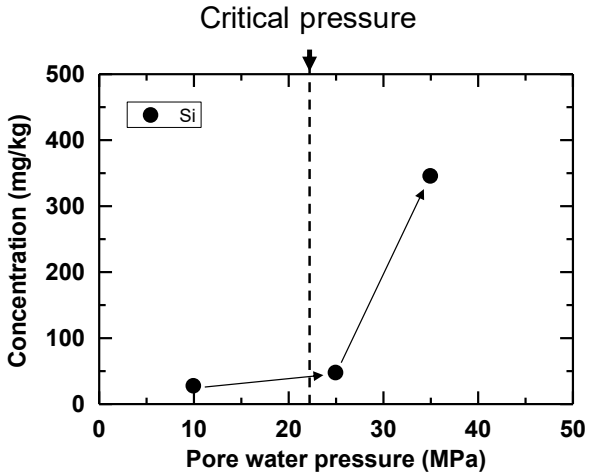

Figure 7: Pore-water-pressure-dependence for Si concentration in free-face dissolution experiments. Arrows approximate the pore-water pressure dependences.

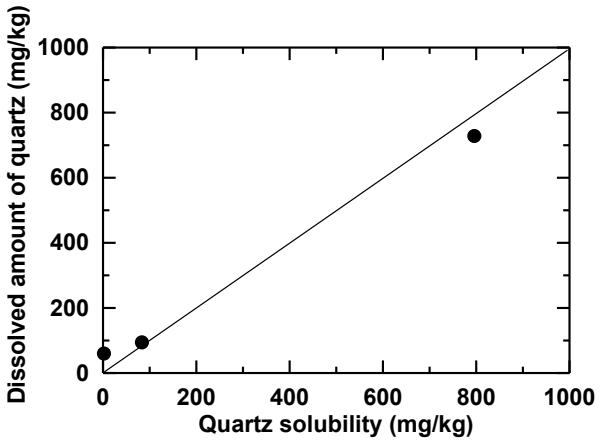

Figure 8: Relation between quartz dissolved in effluent and quartz solubility in free-face dissolution experiments.

Figure 9 shows the relationship between the rate of permeability change and the difference between the quartz concentration in the pore water and its solubility. Note that the concentration in the pore water is assumed to be the average of the quartz concentrations in the injected water (zero) and in the effluent. The effluent concentrations are approximated by the quartz solubility because the two are almost identical as shown in Figure 8. It is clear that the rate of permeability enhancement increases linearly with concentration difference (slope: 5.0×10^{-4} $days^{-1}$ mg^{-1} kg). Assuming that the pore water pressure in superhot geothermal environments can be as high as the hydrostatic pressure (20-40 MPa) corresponding to depths of 2-4 km, quartz solubility can be as high as 1,000 mg/kg, for instance, (i.e., 981 mg/kg at 400°C and 40 MPa) (Manning, 1994). It is therefore possible that permeability enhancement by free-face dissolution could proceed fast enough to counteract the permeability reduction caused by pressure solution or actually enhance permeability even when pressure solution occurs, particularly at a large concentration differences, as discussed below.

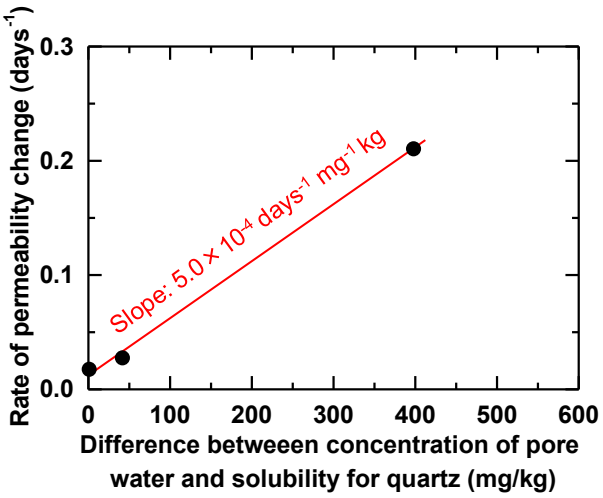

Figure 9: Relation between rate of permeability change and difference between concentration of pore water and solubility for quartz.

3.3 Permeability stabilization/enhancement when pressure solution occurs

When water that is unsaturated for quartz circulates in a superhot EGS, the competition between permeability reduction by pressure solution and permeability enhancement by free-face dissolution gives rise to permeability changes. Assuming that these two processes occur independently, a criterion for permeability stabilization may be determined based on the observed rates of permeability changes they create, which are, respectively, functions of the effective confining stress and the difference between the quartz concentration in the pore water and its solubility.

Based on the present experimental results, the rate of permeability change (reduction) due to pressure solution r_{ps} (day^{-1}) at 400°C may be described by the following equations:

$$r_{ps} = 0 \qquad \text{at } \sigma_{eff} \leq 20 \text{ MPa}, \tag{8}$$

$$r_{ps} = -3.0 \times 10^{-3} \ (\sigma_{eff} - 20) \qquad \text{at } \sigma_{eff} > 20 \text{ MPa}, \tag{9}$$

where the zero-rate below 20 MPa of Eq. 8 is based on the very small permeability changes at 18 MPa (~20 MPa), and the coefficient of Eq. 9 is the slope of a least squares linear regression curve for confining pressures above 18 MPa, as shown in Figure 5. On the other hand, the rate of permeability change (enhancement) by free-face dissolution r_{ffd} (day^{-1}) at 400°C may be described by the following equation:

$$r_{ffd} = 5.0 \times 10^{-4} \ (C_{eq} - C_{pore}), \tag{10}$$

where the coefficient in Eq. 10 is the slope of a least squares linear regression curve for the results at all pore water pressures shown in Figure 9, where a rate of zero is assumed when the concentration difference is zero. From these equations, the concentration difference required to stabilize the permeability for each effective confining stress (i.e., the permeability stabilization criterion) at 400°C may be written as:

$$(C_{eq} - C_{pore}) = 0 \qquad at\ \sigma_{eff} \leq 20 \text{ MPa}, \tag{11}$$

$$(C_{eq} - C_{pore}) = \frac{3.0\times10^{-3}}{5.0\times10^{-4}}(\sigma_{eff} - 20) = 6 \cdot (\sigma_{eff} - 20) \qquad at\ \sigma_{eff} > 20 \text{ MPa}. \tag{12}$$

Here, we discuss whether the permeability stability criterion may be significantly different for different temperatures between 350-500°C or not. That is, we consider how temperature affects Eqs. 11 and 12. At 400°C, pressure solution starts to occur at an effective confining stress of about 20 MPa, providing Eq. 11. Based on the theory, this effective confining stress level may change with temperature as the critical stress is a function of temperature (Eq. 2), where the critical stress for quartz is calculated as approximately 63 MPa at 350°C, 61 MPa at 400°C, and 56 MPa at 500°C. Therefore, the critical stress does not change significantly with temperature, and the effective confining stress level at which pressure solution starts to occur effectively, is approximately constant in the range from 350-500°C. On the other hand, temperature may change the rate of pressure solution (Eq. 1) as the dissolution rate constant is known to be temperature dependent. Additionally, the rate of free-face dissolution may also change with temperature since the same dissolution rate constant appears in Eq. 5. Since the same dissolution rate constant appears in both equations for pressure solution and free-face dissolution, the coefficient in Eq. 12, which corresponds to the ratio of the magnitudes for pressure solution and free-face dissolution, does not change with temperature. Therefore, Eqs. 11 and 12 may be applicable at 350-500°C.

Figure 10 shows the permeability stabilization criterion above/below which permeability enhancement/reduction occurs, where the permeability enhancement and reduction are faster respectively for larger concentration differences and smaller effective confining

stresses, and smaller concentration differences and larger effective confining stresses. As mentioned before, Okamoto et al. (2017) has reported permeability enhancement of fractures in granite at 350°C, effective confining stresses of 20 MPa, and pore water pressure of 20 MPa. Under those conditions, the quartz solubility is about 758 mg/kg (Manning, 1994), and the amount of quartz dissolved in the effluent can be estimated as ca. 366 mg/kg in average. Assuming that the concentration of pore water is the average of the concentrations in the injected water (zero) and the effluent, the concentration difference is 575 mg/kg as the concentration in the pore water is about 183 mg/kg. It is clear that the experimental conditions in Okamoto et al. (2017) are situated in the region of permeability enhancement in Figure 10, supporting the validity of the permeability stability criterion. The figure clearly shows that there is the possibility of stabilizing or even enhancing permeability at concentration differences and effective confining stresses that may occur in combination in superhot EGS.

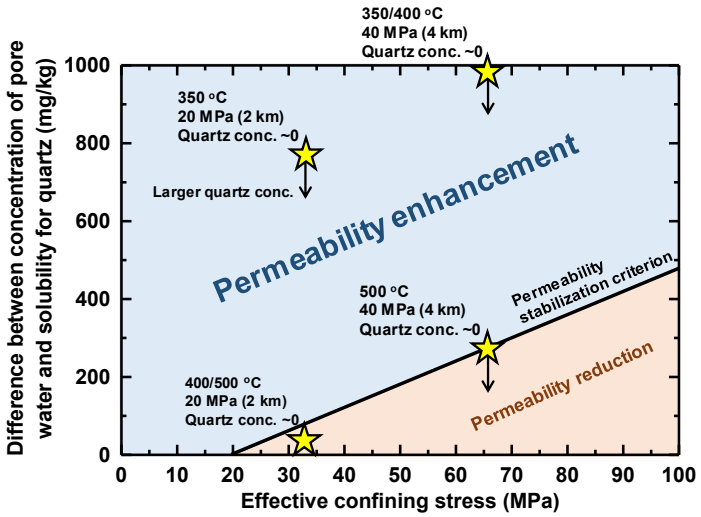

Figure 10: Permeability stabilization criterion above/below which permeability enhancement/reduction occurs. Stars correspond to conditions for different near/super-critical temperatures and pore water pressures approximated by hydrostatic pressures corresponding to the depths indicated on the labels, with quartz concentrations of zero in the pore water at reaction onset. The positions of the stars may drop as the reaction proceeds, as indicated by the arrows.

The stars in the figure correspond to the conditions for different near/super-critical temperatures (i.e., 350, 400 and 500°C) and pore water pressures approximated by hydrostatic pressures of about 20 and 40 MPa at depths of 2 and 4 km, given quartz concentrations of about zero in the pore water at the beginning of the reaction. The positions of the stars may drop as the amount of quartz dissolved in the pore water increases as the reaction proceeds, as indicated by the arrows. The figure clearly illustrates different difficulties for permeability stabilization/enhancement at different temperatures. At near-critical temperatures such as 350°C, at which water is liquid, permeability enhancement may be possible at various effective confining stress levels (i.e., depths) because the concentration difference at the beginning of the reaction, which is approximately equivalent to the quartz solubility, is far from the permeability stabilization criterion. However, at near/super-critical temperatures such as 400°C, when water is vapor or supercritical fluid, the difficulty in stabilizing or enhancing the permeability varies greatly with effective confining stress level. For instance, at 400°C, permeability enhancement may be possible at a pore water pressure of 40 MPa at a depth of 4 km due to the large quartz solubility in such high-pressure supercritical water, whereas only permeability stabilization may be possible at 20 MPa at a depth of 2 km due to quartz's small solubility in vapor. Moreover, at higher supercritical temperatures such as 500°C where quartz solubility is generally low, permeability enhancement is quite challenging. For instance, at 500°C, only permeability stabilization is (perhaps) possible at 20 MPa (2 km deep), whereas even permeability stabilization may be challenging at 40 MPa (4km). In such challenging conditions, generating higher pore water pressures that exceed the naturally occurring hydrostatic pressure would be required so that the stars in the figure move in the upper left direction.

Although it is not so easy to stabilize or enhance the permeability under some conditions that occur in superhot EGS, the present study has clearly shown for the first time that permeability stabilization/enhancement is likely in superhot EGS even when pressure solution occurs by keeping the difference between the quartz concentration in the pore water and its solubility higher than the permeability stabilization criterion. It is therefore worthwhile to further investigate ways to stabilize or enhance permeability in superhot EGS in future studies through, for instance, a superhot geothermal reservoir simulation, together with an experimental validation of the present findings.

4. CONCLUSIONS

The present experimental study aimed to clarify the impacts of pressure solution and free-face dissolution on the permeability of a fracture created in granite. It also investigated the possibility and means of stabilizing/enhancing permeability when pressure solution is present in superhot geothermal systems (EGS) operating at temperatures of 400-500°C and depths of about 2-4 km. Based on the experiments and analyses, we can make the following conclusions. Quartz preferentially dissolves during both pressure solution and free-face dissolution. Pressure solution effectively begins at an effective confining stress of around 20 MPa, and the rate of permeability reduction due to pressure solution (predominantly stress solution) linearly increases with increasing effective confining stress. The rate of permeability enhancement caused by free-face dissolution linearly increases with the difference between concentration of quartz in the pore water and quartz's solubility, and importantly can exceed the rate of permeability reduction at

large concentration differences. Consequently, permeability reduction at a given effective confining stress can be counteracted by permeability enhancement at a specific concentration difference (i.e., permeability stabilization criterion). Additionally, when the concentration difference exceeds the criterion, permeability enhancement is possible even when pressure solution occurs.

ACKNOWLEDGEMENTS

The present study was supported in part by the Japan Society for the Promotion of Science (JSPS) through Grants-in-Aid for Specially Promoted Research (No. 25000009), Scientific Research (B) (No. 17H03504) and Challenging Research (Exploratory) (No. 18K19039). The authors would like to thank Dr. Shinichi Yamasaki at the Graduate School of Environmental Studies, Tohoku University for helping in using ICP-OES, supported by JST/JICA SATREPS (No. JPMJSA1703). The authors also would like to thank Toei Scientific Industrial Co., Ltd. for manufacturing the experimental system. The data that support the findings of this study are available from the corresponding author upon reasonable request. All figures were reprinted from Applied Energy, 260, Watanabe et al., Stabilizing and enhancing permeability for sustainable and profitable energy extraction from superhot geothermal environments, 114306, Copyright (2019), with permission from Elsevier.

REFERENCES

Batini, F. et al. San Pompeo 2 deep well: a high temperature and high pressure geothermal system. In: Strub, A., Ungemach, P., editors. European geothermal update: Proceedings of the 3rd international seminar on the results of EC geothermal energy research, pp. 341–353 (1983).

Baron, G. & Ungemach, P. European geothermal drilling experience-problem areas and case studies. In: International geothermal drilling and completions technology conference. Albuquerque, NM, USA. p. 24 (1981).

Elders, W. A., Friðleifsson, G. & Albertsson, A. Drilling into magma and the implications of the Iceland Deep Drilling project (IDDP) for high-temperature geothermal systems worldwide. Geothermics 49, 111–118 (2014).

Espinosa-Paredes, G. & Garcia-Gutierrez, A. Estimation of static formation temperatures in geothermal wells. Energy Conv. Manag. 44(8), 1343–55 (2003).

Fournier, R. O. The transition from hydrostatic to greater than hydrostatic fluid pressure in presently active continental hydrothermal systems in crystalline rock. Geophys Res Lett. 18(5), 955–958 (1991).

Fournier, R. O. Hydrothermal processes related to movement of fluid from plastic into brittle rock in the magmatic-epithermal environment. Econ. Geol. 94(8), 1193–1211 (1999).

Friðleifsson, G. O., Elders, W. A. & Albertsson, A. The concept of the Iceland Deep Drilling project. Geothermics 49, 2–8 (2014).

Friðleifsson, G. O. & Elders, W. A. The Iceland Deep Drilling project geothermal well at Reykjanes successfully reaches its supercritical target. Geotherm. Resour. Counc. Bull. 46, 30–33 (2017).

Garcia, J. et al. The Northwest Geysers EGS demonstration project, California: Part 1: characterization and reservoir response to injection. Geothermics 63, 97–119 (2016).

Ingason, K., Kristjánsson, V. & Einarsson, K. Design and development of the discharge system of IDDP-1. Geothermics 49, 58–65 (2014).

Ishibashi, T., McGuire, T. P., Watanabe, N., Tsuchiya, N. & Elsworth, D. Permeability evolution in carbonate fractures: Competing roles of confining stress and fluid pH. Water Resour. Res. 49, 2828–2842, doi:10.1002/wrcr.20253 (2013).

Kato, O., Doi, N., Sakagawa, Y. & Uchida, T. Fracture systematics in and around well WD-1, Kakkonda geothermal field, Japan. Geothermics. 27(5–6), 609–29 (1998).

Li, S., Femg, X-T., Zhang, D. & Tang, H. Coupled thermo-hydro-mechanical analysis of stimulation and production for fractured geothermal reservoirs. Appl Energy 247, 40-59 (2019).

Lin, W. Permanent strain of thermal expansion and thermally induced microcracking in Inada granite. J. Geophys. Res 107(B10), 2215, doi:10.1029/2001JB000648 (2002).

Manning, C. E. The solubility of quartz in H2O in the lower crust and upper mantle. Geochim. Cosmochim. Acta. 58 (22), 4831-4839 (1994).

Moore, D. E., Lockner, D. A. & Byerlee, J. D. Reduction of permeability in granite at elevated temperatures. Science 265, 1558–1561 (1994).

Morrow, C. A., Moore, D. E. & Lockner, D. A. Permeability reduction in granite under hydrothermal conditions. J. Geophys. Res. 106, 30551–30560 (2001).

Okamoto, A., Tanaka, H., Watanabe, N., Saishu, H. & Tschiya, N. Fluid pocket generation in response to heterogeneous reactivity of a rock fracture under hydrothermal conditions. Geophys. Res. Lett. 44, 10,306–10,315 (2017).

Reinsch et al. Utilizing supercritical geothermal systems: a review of past ventures and ongoing research activities. Geothermal Energy 5, 16 (2017).

Revil, A. Pervasive pressure-solution transfer: A poro-visco-plastic model. Geophys. Res. Lett. 26(2), 255–258 (1999).

Ruggieri, G. & Gianelli, G. Fluid inclusion data from the Carboli 11 well, Larderello geothermal field, Italy. In: World Geothermal Congress, Italy; pp. 1087–1091 (1995).

Rutter, E. H. The kinetic of rock deformation by pressure solution. Philos. Trans. R. Soc. A 283, 203–219 (1976).

Steingrimsson, B., Gudmundsson, A., Franzson, H. & Gunnlaugsson, E. Evidence of a supercritical fluid at depth in the Nesjavellir field. In: Proceedings, 15th Workshop on Geothermal Reservoir Engineering. Stanford: Stanford University, p. 8 (1990).

Friðleifsson, G. O. & Elders, W. A. The Iceland Deep Drilling project: a search for deep unconventional geothermal resources. Geothermics 34, 269–85 (2005).

Friðleifsson, G.O., Albertsson, A., Stefansson, B., Gunnlaugsson, E. & Adalsteinsson, H. Deep Unconventional Geothermal Resources: a major opportunity to harness new sources of sustainable energy. In: Proceedings, 20th World Energy Conference, Rome. World Energy Council; p. 21 (2007).

Saishu, H., Okamoto, A. & Tsuchiya, N. The significance of silica precipitation on the formation of the permeable-impermeable boundary within earth's crust. Terra Nova 26(4), 253–259 (2014).

Shimizu, I. Kinetics of pressure solution creep in quartz: theoretical considerations. Tectonophysics 245, 121–134 (1995).

Smith, R. & Shaw, H. Igneous-related geothermal systems. In: White, D. and Williams, D., editors. Assessment of geothermal resources of the United States—1975. U.S. Geological Survey Circular 726, 58–83 (1975).

Smith, R. & Shaw, H. Igneous-related geothermal systems. In: Muffler, L., editor. Assessment of geothermal resources of the United States, 1978. U.S. Geological Survey Circular 790, 12–17 (1979).

Stephenson, L. P., Plumley, W. J. & Palciauskas, V. V. A model for sandstone compaction by grain interpenetration, J. Sediment. Petrol. 62, 11–22 (1992).

Takahashi, H., Shoji, T., Nitoh, M & Kojima, T. Effects of water/rock interaction upon crack-like reservoir. J. Geotherm. Res. Soc. Jpn. 10(3), 193–210 (1988).

Tang, Y. W. & Witherspoon, P. A. Hydromechanical behavior of a deformable rock fracture subject to normal stress. J. Geophys. Res. 86, 9287–9298 (1981).

Tester, J. W. et al. The future of geothermal energy in the 21 century impact of enhanced geothermal systems (EGS) on the United States. Cambridge: MIT Press (MA) (2006).

Tsuchiya, N. & Hirano, N. Chemical reaction diversity of geofluids revealed by hydrothermal experiments under sub- and supercritical states. Isl. Arc 16(1), 6–15 (2007).

Tsuchiya, N., Yamada, R. & Uno, M. Supercritical geothermal reservoir revealed by a granite-porphyry system. Geothermics 63, 182–194 (2016).

Tullis, J. & Yund, R. A. Experimental deformation of dry Westerly granite. J. Geophys. Res. 82, 5705–5718 (1977).

Violay, M., Heap, M. J., Acosta, M. & Madonna, C. Porosity evolution at the brittle-ductile transition in the continental crust: Implications for deep hydro-geothermal circulation. Sci. Rep. 7 Article number: 7705 (2017).

Watanabe, N. et al. Potentially exploitable supercritical geothermal resources in the ductile crust. Nat. Geosci. 10(2), 140–144 (2017a).

Watanabe, N., Egawa, M., Sakaguchi, K., Ishibashi, T. & Tsuchiya, N. Hydraulic fracturing and permeability enhancement in granite from subcritical/brittle to supercritical/ductile conditions. Geophys. Res. Lett. 44, 5468–5475 (2017b).

Watanabe, N. et al. Cloud-fracture networks as a means of accessing superhot geothermal energy. Sci. Rep. 9, Article number: 939 (2019).

Weis, P., Driesner, T. & Heinrich, C. A. Porphyry-copper ore shells form at stable pressure-temperature fronts within dynamic fluid plumes. Science 338, 1613–1616 (2012).

Witherspoon, P. A., Wang, J. S. Y., Iwai, K. & Gale, J. E. Validity of cubic law for fluid flow in a deformable rock fracture. Water Resour. Res. 16(6), 1016–1024 (1980).

Yasuhara, H., Elsworth, D. & Polak, A. A mechanistic model for compaction of granular aggregates moderated by pressure solution. J. Geophys. Res. 108(B11), 2530, doi:10.1029/2003JB002536 (2003).

Yasuhara, H. & Elsworth, D. Evolution of permeability in a natural fracture: Significant role of pressure solution. J. Geophys. Res. 109, B03204, doi:10.1029/2003JB002663 (2004).

Yasuhara, H. Spontaneous switching between permeability enhancement and degradation in fractures in carbonate: lumped parameter representation of mechanically and chemically-mediated dissolution. Trans. Porous Media 65, 385–409 (2006).

Yasuhara, H. et al. Temporal alteration of fracture permeability in granite under hydrothermal conditions and its interpretation by coupled chemo-mechanical model. Appl. Geochem. 26, 2074-2088 (2011).